

# Studies of earth shielding effect to direct dark matter searches at the China Jinping Underground Laboratory

Z. Z. Liu,<sup>1</sup> L. T. Yang,<sup>1,\*</sup> Q. Yue,<sup>1,†</sup> C. H. Yeh,<sup>2,‡</sup> K. J. Kang,<sup>1</sup> Y. J. Li,<sup>1</sup> M. Agartioglu,<sup>2,‡</sup> H. P. An,<sup>1,3</sup> J. P. Chang,<sup>4</sup> J. H. Chen,<sup>2,‡</sup> Y. H. Chen,<sup>5</sup> J. P. Cheng,<sup>1,6</sup> W. H. Dai,<sup>1</sup> Z. Deng,<sup>1</sup> C. H. Fang,<sup>7</sup> X. P. Geng,<sup>1</sup> H. Gong,<sup>1</sup> X. Y. Guo,<sup>5</sup> Q. J. Guo,<sup>8</sup> L. He,<sup>4</sup> S. M. He,<sup>5</sup> J. W. Hu,<sup>1</sup> H. X. Huang,<sup>9</sup> T. C. Huang,<sup>10</sup> H. T. Jia,<sup>7</sup> X. Jiang,<sup>7</sup> H. B. Li,<sup>2,‡</sup> H. Li,<sup>4</sup> J. M. Li,<sup>1</sup> J. Li,<sup>1</sup> R. M. J. Li,<sup>7</sup> X. Li,<sup>9</sup> X. Q. Li,<sup>11</sup> Y. L. Li,<sup>1</sup> B. Liao,<sup>6</sup> F. K. Lin,<sup>2,‡</sup> S. T. Lin,<sup>7</sup> S. K. Liu,<sup>7</sup> Y. Liu,<sup>7</sup> Y. D. Liu,<sup>6</sup> Y. Y. Liu,<sup>6</sup> H. Ma,<sup>1</sup> Y. C. Mao,<sup>8</sup> Q. Y. Nie,<sup>1</sup> J. H. Ning,<sup>5</sup> H. Pan,<sup>4</sup> N. C. Qi,<sup>5</sup> J. Ren,<sup>9</sup> X. C. Ruan,<sup>9</sup> V. Sharma,<sup>2,12,‡</sup> Z. She,<sup>1</sup> K. Saraswat,<sup>2,‡</sup> M. K. Singh,<sup>2,12,‡</sup> T. X. Sun,<sup>6</sup> C. J. Tang,<sup>7</sup> W. Y. Tang,<sup>1</sup> Y. Tian,<sup>1</sup> G. F. Wang,<sup>6</sup> L. Wang,<sup>13</sup> Q. Wang,<sup>1,3</sup> Y. Wang,<sup>1,3</sup> Y. X. Wang,<sup>8</sup> Z. Wang,<sup>7</sup> H. T. Wong,<sup>2,‡</sup> S. Y. Wu,<sup>5</sup> Y. C. Wu,<sup>1</sup> H. Y. Xing,<sup>7</sup> Y. Xu,<sup>11</sup> T. Xue,<sup>1</sup> Y. L. Yan,<sup>7</sup> N. Yi,<sup>1</sup> C. X. Yu,<sup>11</sup> H. J. Yu,<sup>4</sup> J. F. Yue,<sup>5</sup> M. Zeng,<sup>1</sup> Z. Zeng,<sup>1</sup> F. S. Zhang,<sup>6</sup> Z. Y. Zhang,<sup>1</sup> M. G. Zhao,<sup>11</sup> J. F. Zhou,<sup>5</sup> B. T. Zhang,<sup>1</sup> K. K. Zhang,<sup>7</sup> Z. H. Zhang,<sup>1</sup> Z. Y. Zhou,<sup>9</sup> and J. J. Zhu<sup>7</sup>

(CDEX Collaboration)

<sup>1</sup>Key Laboratory of Particle and Radiation Imaging (Ministry of Education) and Department of Engineering Physics, Tsinghua University, Beijing 100084

<sup>2</sup>Institute of Physics, Academia Sinica, Taipei 11529

<sup>3</sup>Department of Physics, Tsinghua University, Beijing 100084

<sup>4</sup>NUCTECH Company, Beijing 100084

<sup>5</sup>YaLong River Hydropower Development Company, Chengdu 610051

<sup>6</sup>College of Nuclear Science and Technology, Beijing Normal University, Beijing 100875

<sup>7</sup>College of Physics, Sichuan University, Chengdu 610065

<sup>8</sup>School of Physics, Peking University, Beijing 100871

<sup>9</sup>Department of Nuclear Physics, China Institute of Atomic Energy, Beijing 102413

<sup>10</sup>Sino-French Institute of Nuclear and Technology, Sun Yat-sen University, Zhuhai, 519082

<sup>11</sup>School of Physics, Nankai University, Tianjin 300071

<sup>12</sup>Department of Physics, Banaras Hindu University, Varanasi 221005

<sup>13</sup>Department of Physics, Beijing Normal University, Beijing 100875

(Dated: November 23, 2021)

Dark matter direct detection experiments mostly operate at deep underground laboratory. It is necessary to consider shielding effect of the earth, especially for strongly interacting massive particle dark matter. We analyzed and simulated the earth shielding effect for dark matter at the China Jinping Underground Laboratory (CJPL) with a simulation package, CJPL Earth Shielding Simulation code (CJPL\_ESS) which is applicable to other underground locations. The further constraints on the  $\chi$ -N cross-section exclusion regions are derived based on the studies with CDEX experiment data.

**PACS numbers:** 95.35.+d, 29.40.-n, 98.70.Vc

*Introduction.* Weakly interacting massive particles (WIMPs) as a dark matter candidate, denoted as  $\chi$ , have not been accurately observed in direct detection experiments, the results of which are expressed with exclusion plots showing the upper limits [1–5]. Direct detection experiments are mostly located in deep underground laboratory, such as CJPL [6], SNOlab [7], LNGS [8], which means that the dark matter particle will go through at least several kilometers of rock before reaching the laboratory. Generally, the transport of dark matter will not be affected by rocks, but the shielding effect may not be negligible for large cross section dark matter. Therefore, the flux of dark matter at laboratory will be greatly suppressed at large cross section. This phenomenon is called earth shielding effect, having been studied in detail in [9–12].

According to [9–12], the event rate of WIMP-nucleus ( $\chi$ -N) scattering will decrease as the cross section in-

creases at large cross section. That means constraints of  $\chi$ -N cross section is not an upper limit, but an exclusion region. The direct detection experiments at underground laboratory cannot detect dark matter with a too large  $\chi$ -N cross section, due to the shielding effect of overburden. Ref. [9–12] have studied the shielding effect in detail, but the simulation object is the entire earth, which is actually more suitable for underground laboratories in mine, such as SNOlab, and not completely suitable for laboratories at traffic tunnel whose overburden are mountain, such as CJPL, LNGS. In this paper, we analyzed and simulated the earth shielding effect for dark matter at CJPL, and we also calculated the exclusion region of  $\chi$ -N cross section with CDEX [1, 13–20] experiment data.

*Theory.* Typically, dark matter interacts with target nucleus via elastic scattering, and after scattering, the dark matter particle loses part of its kinetic energy and the movement direction of the particle is bent. While

dark matter particles go through the mountain rocks, they are bent and slowed down, so their tracks are no longer straight lines but broken lines. Consequently, simulation that only energy loss taken into account is not completely in line with the actual transport process, a complete Monte Carlo (MC) simulation based on  $\chi$ -N scattering is necessary.

Mean free path (denoted as  $\lambda$ ) is a key parameter for MC simulation. The overburden contains multiple nuclides, so the mean free path can be expressed as

$$\frac{1}{\lambda} = \sum_i \frac{f_i \rho}{m_{A_i}} \sigma_{\chi A_i}, \quad (1)$$

where  $\rho$  is the density of the transport medium,  $f_i$  is the mass fraction of the  $i_{th}$  nuclide in transport medium,  $m_{A_i}$  is the mass of the  $i_{th}$  nuclide, and  $\sigma_{\chi A_i}$  is cross section of  $\chi$ - $A_i$  scattering, where  $A_i$  refers to nucleus of the  $i_{th}$  nuclide. For low mass dark matter whose mass  $m_\chi$  is less than  $10 \text{ GeV}/c^2$ , the form factor  $F(q) \sim 1$ , where  $q$  is equal to  $\sqrt{2m_A E_R}$ ,  $E_R$  is nuclear recoil energy. In this way,  $\sigma_{\chi A_i}^{SI}$  is equal to  $\sigma_{\chi N}^{SI}(0) \frac{\mu_{\chi A_i}^2}{\mu_{\chi n}^2} A_i^2$  for  $\chi$ -N spin-independent (SI) scattering, where  $\sigma_{\chi N}^{SI}$  refers to  $\chi$ -nucleon SI-interactions cross section,  $\mu$  refers to reduced mass. The mean free path of  $\chi$  at Jinping Mountain in SI-scattering process was shown in Fig 1, where the blue line is that of cross section at  $10^{-30} \text{ cm}^2$ , and the orange line is that of cross section at  $10^{-31} \text{ cm}^2$ . At the same cross section, the mean free path decreases with the increase of  $\chi$ 's mass. Before every scattering, the free path of dark matter particle can be calculated by

$$l = -\lambda \ln(1 - \xi), \quad (2)$$

where  $\xi$  follows an uniform distribution between 0 to 1, denoted as  $\xi \sim U(0, 1)$ .

The  $\chi$ -N scattering is treated as elastic scattering process. In the center of mass coordinate frame, the magnitude of  $\chi$ 's velocity remains the same in scattering process, which is expressed as  $v_{\chi c} = v'_{\chi c}$ , where  $v_{\chi c}$  refers to the velocity of  $\chi$  in Center of Mass (CMS) frame before scattering,  $v'_{\chi c}$  refers to the velocity of  $\chi$  in CMS frame after scattering. In laboratory frame, the velocity of  $\chi$  after scattering is

$$\vec{v}'_\chi = v_{\chi c} \vec{n} + \vec{v}_c, \quad (3)$$

where  $\vec{v}_c$  is the velocity of CMS frame in lab frame,  $\vec{n}$  is the direction of  $\chi$  after scattering in CMS frame. The direction of  $\chi$  after scattering is isotropic in CMS frame, so the scattering angle  $\cos\alpha \sim U(-1, 1)$ . The scattering angle  $\theta$  in lab frame can be calculated by

$$\tan\theta = \frac{\sin\alpha}{\cos\alpha + \frac{m_\chi}{m_A}}, \quad (4)$$

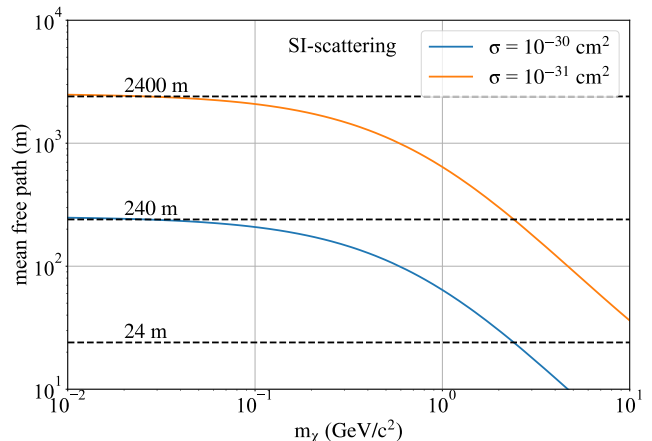


FIG. 1. The mean free path of  $\chi$  at Jinping Mountain in SI-scattering process, the blue line is that of cross section at  $10^{-30} \text{ cm}^2$ , and the orange line is that of cross section at  $10^{-31} \text{ cm}^2$ . The density of the transport medium is set to be  $2.7 \text{ g/cm}^3$ , and the composition of the transport medium is adopted as Table I. At the same cross section, the mean free path decreases with the increase of  $\chi$ 's mass.

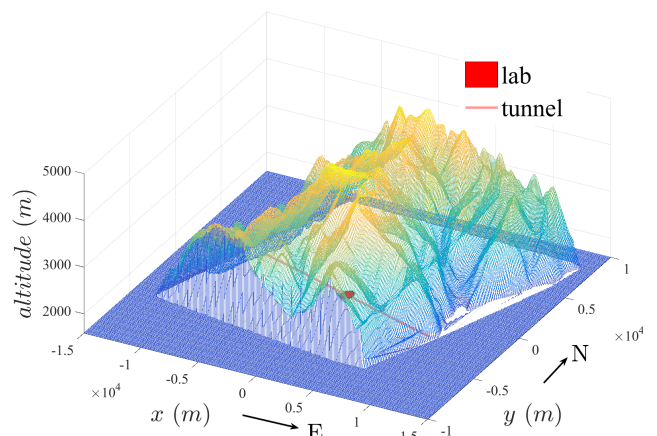


FIG. 2. The topographic map of Jinping Mountain, where the red solid line represents the tunnel, the red circular area represents the laboratory. The contour data is obtained from Google Maps. The altitude of the laboratory is about 1600 m, and the highest point of Jinping Mountain is about 4000 m. The coordinate of the laboratory is at  $(0, 0, 1590 \text{ m})$ , and the x-axis points to the east, the y-axis points to the north, and the z-axis points upward.

TABLE I. The main compositions of the rocks of Jinping Mountain, where  $f$  represents the mass fraction. The rock is marble, the main component is  $\text{CaCO}_3$ , and the most abundant nuclides are O, Ca, Mg and C.

element	O	Ca	Mg	C	Si	Al	Fe	K	Na	P
$f$ (%)	46.42	31.96	11.50	9.59	0.19	0.15	0.10	0.07	0.01	0.01
Z	8	20	12	6	14	13	26	19	11	15
A	16	40	24	12	28	27	56	39	23	31

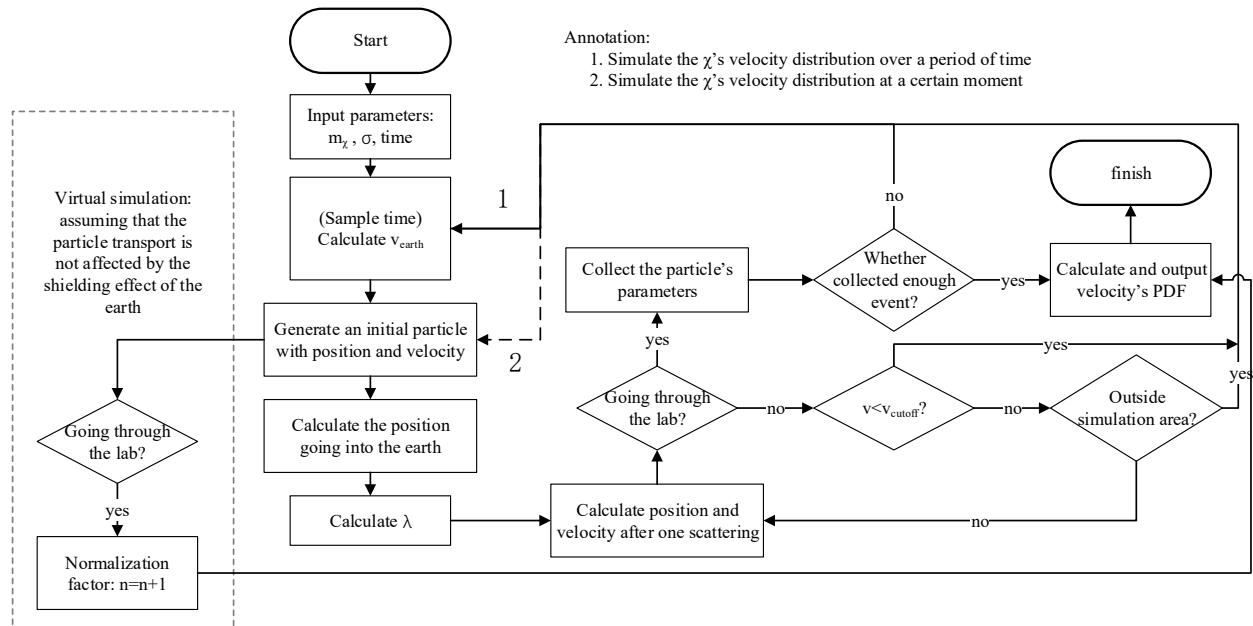


FIG. 3. The flow chart of CJPL\_ESS code. The “virtual simulation” module serves calculating the number of particles reaching the lab without earth shielding effect, which can be applied as normalization factor when calculate  $\chi$ 's velocity distribution. Parallel computing based on Message Passing Interface (MPI) and bias sampling method have been used to speed up the program running time. The program has two routes, following route 1 can simulate the  $\chi$ 's velocity distribution over a period of time, and following route 2 can simulate the  $\chi$ 's velocity distribution at a certain moment.

*Simulation.* CJPL is located at the center of a traffic tunnel under Jinping mountain in Sichuan province, southwest China, where the latitude and longitude is approximately (E101.7°, N28.2°). The length of the tunnel is about 17.5 km, and the rock overburden at CJPL is about 2400 m vertically. The altitude of the laboratory is about 1600 m, and the highest point of Jinping mountain is about 4000 m [6]. The topographic map of Jinping Mountain is shown in Fig. 2. The rocks of Jinping Mountain are mainly marble, whose density is about 2.7 g/cm<sup>3</sup>, and the main elements include are O, Ca, Mg, C. On the basis of the test result of ore composition, the detailed composition of the rocks is shown in Table. I.

It can be easily inferred that for these dark matter particles reaching the lab, that traveling from below will travel much farther distance in the earth than that traveling from above. The particles traveling from below is negligible in simulation at large cross section. Based on this assumption, an earth shielding effect simulation program for CJPL laboratory (or any underground laboratory under mountain) was developed, which is mainly suitable for the simulation of dark matter at large cross section or with mean free path less than several kilometers. The program is named CJPL laboratory Earth Shielding effect Simulation code (denoted as CJPL\_ESS).

In CJPL\_ESS simulation framework, coordinate sys-

tem is established with the laboratory stationary and as the origin. The initial dark matter particles are uniformly generated on a square plane of 100 km×100 km, 3 km above the laboratory. The initial velocity is got by

$$\vec{v}_{\chi,lab} = \vec{v}_{\chi,gal} - \vec{v}_{lab}, \quad (5)$$

where  $\vec{v}_{\chi,gal}$  is the velocity in galaxy, the distribution of which follows Maxwell distribution [21],  $\vec{v}_{lab}$  is the velocity of laboratory in galaxy, which is equal to  $\vec{v}_{earth} + \vec{v}_{rot}$ ,  $\vec{v}_{earth}$  is the velocity of earth,  $\vec{v}_{rot}$  is the velocity of the earth's rotation at laboratory.  $\vec{v}_{lab}$  is related to sidereal time and the latitude and longitude of the laboratory, which can be calculated as Ref. [22]. Particles are collected on a horizontal plane with a radius of 500 meters centered on the laboratory, and the particle that went through the plane are counted to calculate the velocity distribution. The flow chart of CJPL\_ESS code is shown in Fig. 3, and the code can output the velocity distribution of  $\chi$  at CJPL with a given  $m_\chi$ ,  $\sigma_{\chi N}$  and time (or a period of time). Parallel computing based on Message Passing Interface (MPI) and bias sampling method have been used to speed up the program running time.

According to Eq. 4, the direction of dark matter could be bent by a large angle after every scattering, especially for light dark matter. Consequently, the track is a tortuous broken line. The track of two simulated events are

shown in Fig. 4. The particle at  $m_\chi$  of  $0.05 \text{ GeV}/c^2$  and SI cross section of  $10^{-30} \text{ cm}^2$  reached the lab after hundreds of scatterings, that is because the particle can only lose a small part of its total kinetic energy by each scattering, and the maximum rate of energy loss at each scattering is  $4\mu_N/m_N$ . In this way, the direction of particle at lab has a very weak correlation with the initial direction, and the distance travelled is much greater than the displacement.

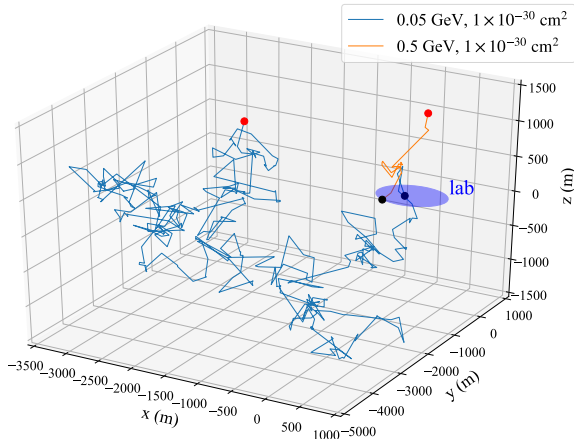


FIG. 4. The simulated track (SI-scattering) of  $\chi$  travelling in mountain. The location of the laboratory is at the origin. The orange line is the track of  $\chi$  at mass of  $0.5 \text{ GeV}$  and cross section of  $1 \times 10^{-30} \text{ cm}^2$ , and the blue line is the track of  $\chi$  at mass of  $0.05 \text{ GeV}$  and cross section of  $1 \times 10^{-30} \text{ cm}^2$ . According to blue line, light dark matter can reach the lab even after several hundreds of scattering.

Using CJPLESS code, we simulated the velocity distribution of  $\chi$  at different masses and cross section at CJPL. The velocity distributions of  $\chi$  at mass of  $0.2 \text{ GeV}/c^2$  and different cross section are shown in Fig. 5. As  $\sigma_{\chi N}^{SI}$  increases from  $1 \times 10^{-32} \text{ cm}^2$  to  $4 \times 10^{-30} \text{ cm}^2$ , the total flux of dark matter particles at lab is getting smaller and smaller.

*Result.* CDEX experiment is located at CJPL, and committed to searching dark matter with high purity germanium detector [1, 13–20]. CDEX-1B data and CDEX-10 data are used to earth shielding effect analysis in this paper. CDEX-1B experiment has for its target a single-element p-type point contact germanium (PPCGe) detector cooled by cold finger, with an active mass of 939 g. A shielding system was built to shield the background radiation from outside the detector, constructed with 20 cm copper, 20 cm PE and 20 cm lead [17]. Different from CDEX-1B, CDEX-10 experiment used three triple-element pPCGe strings (C10A, B, C) directly immersed in liquid nitrogen ( $\text{LN}_2$ ), and the shielding system was constructed with  $\text{LN}_2$  and 20 cm copper [1]. Compared to that of the overburden, the shielding effect of manually built shielding system to dark matter is negligible,

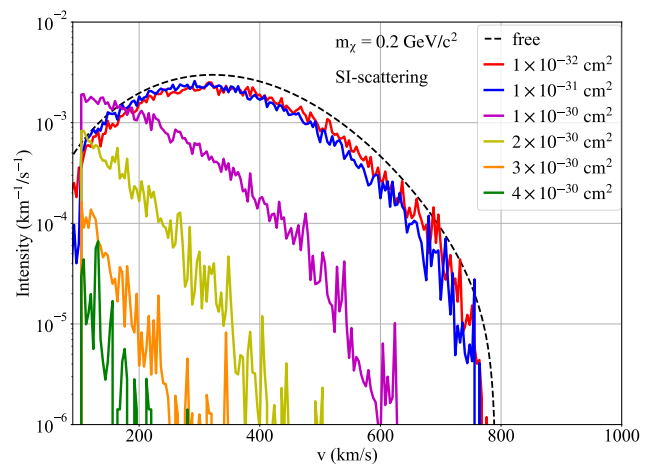


FIG. 5. The velocity distribution of  $\chi$  at mass of  $0.2 \text{ GeV}$  in SI-scattering case. The black dashed line is velocity distribution of  $\chi$  without earth shielding effect taken into account, and the solid lines are that at different SI cross section. In simulation, cutoff velocity of particle was set to be  $100 \text{ km/s}$ .

and has been disregarded in simulation process.

In this work, both  $\chi$ -N elastic scattering and  $\chi$ -N inelastic scattering via migdal effect [23–25] are taken into account. The event rate of  $\chi$ -N elastic scattering is expressed as

$$\frac{dR}{dE_R} = N_T \frac{\rho_\chi}{m_\chi} \int dv v f_v(v, \sigma) \frac{d\sigma}{dE_R}, \quad (6)$$

where  $E_R$  is the nuclear recoil energy,  $N_T$  is the number of target nuclei per unit detector mass,  $\rho_\chi$  is the density of dark matter,  $m_\chi$  is the mass of  $\chi$ ,  $v$  is the velocity of  $\chi$  in lab frame,  $f_v(v, \sigma)$  is velocity distribution of  $\chi$ , which is the output of CJPLESS code. Considering  $\chi$ -N SI scattering and spin-dependent (SD) scattering, the differential cross section can be expressed as

$$\frac{d\sigma}{dE_R} = \frac{m_A}{2\mu_{\chi A}^2 v^2} (\sigma_{\chi A}^{SI} F_{SI}^2(E_R) + \sigma_{\chi A}^{SD} F_{SD}^2(E_R)), \quad (7)$$

where  $\mu_{\chi A}$  refers to reduced mass between  $\chi$  and nucleus A,  $\sigma_{\chi A}^{SI}$  and  $\sigma_{\chi A}^{SD}$  are SI (SD) cross section between  $\chi$  and A, F is the form factor. We will discuss the SI-scattering and SD-scattering case separately later.

Following ref. [25], the event rate of  $\chi$ -N inelastic scattering via migdal effect is calculated by

$$\frac{dR}{dE_{det}} = N_T \frac{\rho_\chi}{m_\chi} \int dv dE_{EM} dE_R \delta(E_{det} - Q_{nr} E_R - E_{EM}) v f_v(v, \sigma) \frac{d\sigma}{dE_{EM} dE_R}, \quad (8)$$

where  $E_{det}$  refers to the energy CDEX PPCGe detectors can detect, which is equal the summation of nuclear recoil energy and electron recoil energy, denoted as  $Q_{nr} E_R + E_{EM}$ , where  $Q_{nr}$  is the quenching factor and was treated following ref. [25].

Considering SI-scattering, the expected energy spectrum at  $\chi$  of different mass and cross section have been calculated using Eq. (6) and (8). The standard WIMP galactic halo assumption and conventional astrophysical models are used, with  $\chi$ -density  $\rho_\chi$  set to  $0.3 \text{ GeV/cm}^3$  [21]. The energy spectrum at mass of  $0.2 \text{ GeV}/c^2$  with different SI cross section are shown in Fig 6. As SI cross section increasing from  $\sim 10^{-32} \text{ cm}^2$  to  $\sim 10^{-30} \text{ cm}^2$ , the count rate of  $\chi$ -N scattering event increases first and then decreases, and decreases sharply at cross section from  $2 \times 10^{-30}$  to  $4 \times 10^{-30} \text{ cm}^2$ . Migdal effect has not been taken into account in earth shielding effect simulation, due to the extremely small incidence rate compared to elastic scattering. For example, at  $m_\chi = 0.2 \text{ GeV}/c^2$ , the ratio for mean energy loss of each  $\chi$ -N scattering via migdal effect to that of  $\chi$ -N elastic scattering is  $\sim 20:1$ , and the ratio of event rate is  $\sim 1:20000$ , the combined ratio of (energy loss  $\times$  event rate) is  $\sim 1:1000$ .

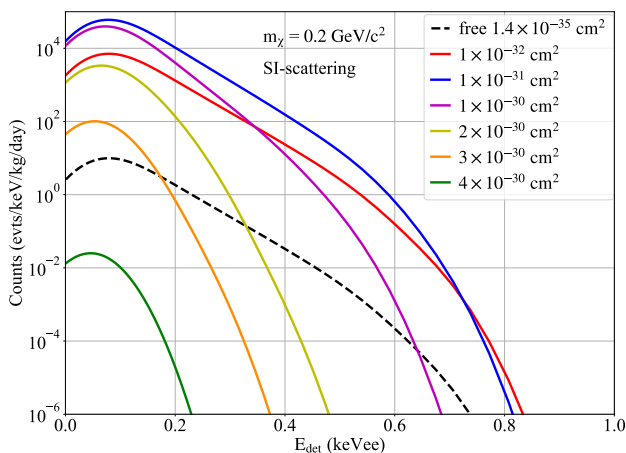


FIG. 6. The energy spectrum of  $\chi$ -N SI inelastic scattering via migdal effect at  $\chi$ -mass of  $0.2 \text{ GeV}/c^2$  in high purity germanium detector, where the SI cross section increases from  $\sim 10^{-32} \text{ cm}^2$  to  $\sim 10^{-30} \text{ cm}^2$ . The black dashed line is the energy spectrum at cross section on  $1.4 \times 10^{-35} \text{ cm}^2$  without earth shielding effect taken into account, the solid lines are the energy spectrum at cross section from  $1 \times 10^{-32}$  to  $4 \times 10^{-30} \text{ cm}^2$ . The energy resolution is taken into account, the standard deviation of which is  $33.5 + 13.2 \times E^{\frac{1}{2}}$  (eV), where  $E$  is expressed in keV.

The exclusion region at 90% confidence level was calculated with CDEX-1B and CDEX-10 data, using binned Poisson method [29] and unified approach [30], respectively. The results are shown in Fig. 7 (a). Although the background and lower limit of the CDEX-1B and CDEX-10 are different, the upper limit of exclusion region of the two experiments are consistent, that's because the count rate of  $\chi$ -N scattering decreases rapidly as  $\sigma_{\chi N}^{SI}$  increase to approach the upper limit. In this way, the upper limit of the exclusion region in Fig. 7 can basically represent the largest cross section of dark matter that can be de-

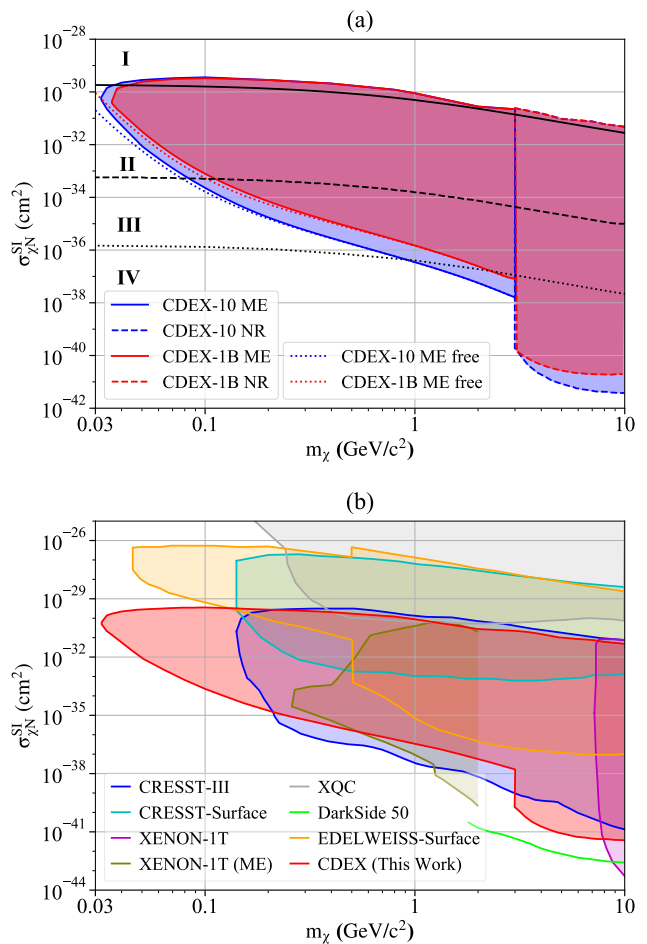


FIG. 7. (a) The exclusion region at 90% confidence level with earth shielding effect considered, derived by CDEX data [1, 17]. The red region enveloped by solid line is the exclusion region on  $\chi$ -N scattering via migdal effect derived by CDEX-1B data, and the blue region enveloped by blue solid line is that derived by CDEX-10 data. Corresponding, the regions enveloped by dashed line are the exclusion regions on  $\chi$ -N elastic scattering derived by CDEX data. The dotted lines are the constraints without earth shielding effect. The red region and blue region have the same upper limit. The black solid line, black dashed line and black dotted line divide the parameter space of  $\chi$  into 4 regions. Region-I is where the cross-sections are so large that no WIMPs ( $<1\%$  in flux) would survive. Regions-II and -III are where upward WIMPs from below would be suppressed completely (survival  $<1\%$ ) or partially (survival 1-99%), respectively. In Region-IV, more than 99% of the upward WIMPs (and therefore all downward ones) would arrive at CJPL, such that the earth effects can be neglected. (b) Summary of results from experiments with published exclusion regions from interaction upper limits and earth attenuation effects, including EDELWEISS [26], CRESST [27], XENON-1T [27, 28] and CDEX. The upper boundary of “XENON-1T (ME)” is lower than that of CDEX is because Ref. [28] adopted a more conservative calculation method.

tected by all experiments at CJPL. And due to the mean free path decreasing as  $m_\chi$  increase, heavier dark matter has lower value of the upper limit of exclusion region.

The typical displacement traversed on earth of the downward-going WIMPs reaching the laboratory is 2.4 -  $\sim 10$  km, while that of the upward WIMPs is  $\sim 100$  - 12800 km. According to simulation, the survival fraction of the WIMPs decreases by a factor of 10 for every additional  $2.3 \lambda$  of distance traveled in the earth's interior. To illustrate at different domains of WIMPs survival to reach CJPL from the “upper” (downward-going) and “lower” (upward-going) hemispheres due to earth shielding effects, Figure 7(a) is further categorized into four regions. Region-I is where the cross-sections are so large that no WIMPs ( $<1\%$  in flux) would survive. Regions-II and -III are where upward WIMPs from below would be suppressed completely (survival  $<1\%$ ) or partially (survival 1-99%), respectively. In Region-IV, more than 99% of the upward WIMPs (and therefore all downward ones) would arrive at CJPL, such that the earth effects can be neglected. We have not considered earth shielding effect at  $\sigma_{\chi N}^{\text{SI}} > 10^{-33} \text{ cm}^2$  (Regions-III and -IV) when calculated the exclusion region. The estimated systematic uncertainties for the earth attenuation simulations in Regions (I,II,III,IV) are ( $\ll 1\%$ ,  $<1\%$ ,  $1\% - 30\%$ ,  $<1\%$ ), respectively. The value “30%” is the total proportion of  $\chi$  from below. The systematic error has been corrected by the integral survival rate of WIMPs from below CJPL and was taken into account in the derivation of the exclusion contours of Fig. 7 (a).

The earth shielding effect of  $\chi$ -N SD scattering has also been simulated and evaluated.  $^{27}\text{Al}$ ,  $^{25}\text{Mg}$  and  $^{13}\text{C}$  in the mountain rocks which are the odd-even nucleus with the largest mass fraction have been considered, and the spin expectation values,  $\langle S_n \rangle$  and  $\langle S_p \rangle$ , follow Ref. [31]. The constraints of neutron-only case was calculated and shown in Fig. 8. The proton-only case has not been considered, because the expectation value,  $\langle S_p \rangle$ , of  $^{73}\text{Ge}$  approaches zero. The spin expectation values used in SD analysis are shown in Table. II.

TABLE II. The spin expectation values used in SD analysis.

Element	Location	Z	A	$\langle S_p \rangle$	$\langle S_n \rangle$	J
C	rock	6	13	-0.009	-0.172	1/2
Mg	rock	12	25	0.04	0.376	5/2
Al	rock	13	27	0.343	0.0296	5/2
Ge	detector	32	73	0.030	0.378	9/2

*Discussion.* In this paper, we have introduced a MC simulation code for earth shielding effect. The code was based on  $\chi$ -N elastic scattering and developed to be applied to simulate the earth shielding effect of CJPL (or other underground laboratory that is under mountain). This simulation package is applicable to other underground locations, after revising the input parameters on topography and compositions. The data of CDEX exper-

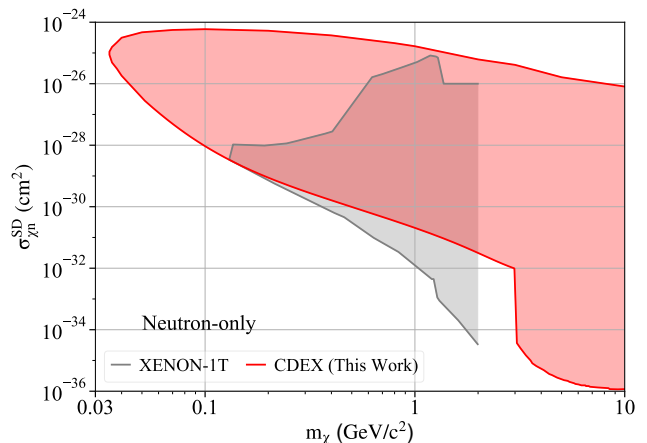


FIG. 8. The exclusion region on  $\chi$ -N SD-scattering of neutron-only case at 90% confidence level with earth shielding effect considered, derived by CDEX data [1]. The momentum-transfer-dependent spin-structure function of  $^{73}\text{Ge}$  was taken from Ref. [32]. The constraint of XENON-1T was taken from Ref. [28], where a more conservative calculation method has been adopted in evaluation of earth shielding effect.

iment at CJPL are used in analysis and new constraints on  $\chi$ -N SI-scattering and SD-scattering with earth shielding effect taken into account were achieved.

This work was supported by the National Key Research and Development Program of China (Grant No. 2017YFA0402200) and the National Natural Science Foundation of China (Grants No. 12175112, No. 12005111, No. 11725522, No. 11675088, No.11475099).

\* Corresponding author: yanglt@mail.tsinghua.edu.cn

† Corresponding author: yueq@mail.tsinghua.edu.cn

‡ Participating as a member of TEXONO Collaboration

- [1] H. Jiang *et al.* (CDEX Collaboration), Phys. Rev. Lett. **120**, 241301 (2018).
- [2] P. Agnes *et al.* (DarkSide Collaboration), Phys. Rev. Lett. **121**, 081307 (2018).
- [3] R. Agnese *et al.* (SuperCDMS Collaboration), Phys. Rev. D **97**, 022002 (2018).
- [4] D. S. Akerib *et al.* (LUX Collaboration), Phys. Rev. Lett. **118**, 021303 (2017).
- [5] E. Aprile *et al.* (XENON Collaboration), Phys. Rev. Lett. **121**, 111302 (2018).
- [6] J. P. Cheng *et al.*, Annu. Rev. Nucl. Part. Sci. **67**, 231 (2017).
- [7] F. Duncan, A. Noble, and D. Sinclair, Annu. Rev. Nucl. Part. Sci. **60**, 163 (2010).
- [8] Gran Sasso National Laboratory, <https://www.lngs.infn.it/en>.
- [9] T. Emken and C. Kouvaris, J. Cosmol. Astropart. Phys. **10**, 031 (2017).
- [10] D. Hooper and S. D. McDermott, Phys. Rev. D **97**, 115006 (2018).

- [11] T. Emken and C. Kouvaris, *Phys. Rev. D* **97**, 115047 (2018).
- [12] B. J. Kavanagh, *Phys. Rev. D* **97**, 123013 (2018).
- [13] S. K. Liu *et al.* (CDEX Collaboration), *Phys. Rev. D* **90**, 032003 (2014).
- [14] W. Zhao *et al.* (CDEX Collaboration), *Phys. Rev. D* **88**, 052004 (2013).
- [15] Q. Yue *et al.* (CDEX Collaboration), *Phys. Rev. D* **90**, 091701 (2014).
- [16] W. Zhao *et al.* (CDEX Collaboration), *Phys. Rev. D* **93**, 092003 (2016).
- [17] L. T. Yang *et al.* (CDEX Collaboration), *Chin. Phys. C* **42**, 23002 (2018).
- [18] L. T. Yang *et al.* (CDEX Collaboration), *Phys. Rev. Lett.* **123**, 221301 (2019).
- [19] H. Jiang *et al.* (CDEX Collaboration), *Sci. China-Phys. Mech. Astron* **62**, 031012 (2018).
- [20] Y. Wang *et al.* (CDEX Collaboration), *Sci. China Phys. Mech. Astron.* **64**, 281011 (2021).
- [21] G. Jungman, M. Kamionkowski, and K. Griest, *Phys. Rep.* **267**, 195 (1996).
- [22] C. McCabe, *J. Cosmol. Astropart. Phys.* **2014**, 027 (2014).
- [23] M. Ibe, W. Nakano, Y. Shoji, and K. Suzuki, *J. High Energy Phys.* **03**, 194 (2018).
- [24] M. J. Dolan, F. Kahlhoefer, and C. McCabe, *Phys. Rev. Lett.* **121**, 101801 (2018).
- [25] Z. Z. Liu *et al.* (CDEX Collaboration), *Phys. Rev. Lett.* **123**, 161301 (2019).
- [26] E. Armengaud *et al.* (EDELWEISS Collaboration), *Phys. Rev. D* **99**, 082003 (2019).
- [27] T. Emken, R. Essig, C. Kouvaris, and M. Sholapurkar, *J. Cosmol. Astropart. Phys.* **2019**, 070 (2019).
- [28] E. Aprile *et al.* (XENON Collaboration), *Phys. Rev. Lett.* **123**, 241803 (2019).
- [29] C. Savage *et al.*, *J. Cosmol. Astropart. Phys.* **04**, 010 (2009).
- [30] G. J. Feldman and R. D. Cousins, *Phys. Rev. D* **57**, 3873 (1998).
- [31] V. A. Bednyako and F. Imkovic, *Physics of Particles and Nuclei* **36**, 131 (2005).
- [32] V. I. Dimitrov, J. Engel, and S. Pittel, *Phys. Rev. D* **51**, R291 (1995).